Langmuir

Invited Feature Article

pubs.acs.org/Langmuir

Designing Synthetic Microcapsules That Undergo Biomimetic Communication and Autonomous Motion

Victor V. Yashin,[†] German V. Kolmakov,[‡] Henry Shum,[†] and Anna C. Balazs*[,†]

[†]Chemical Engineering Department, University of Pittsburgh, Pittsburgh, Pennsylvania 15261, United States

[‡]Physics Department, New York City College of Technology, Brooklyn, New York 11201, United States

ABSTRACT: Inspired by the collective behavior of slime molds and amoebas, we designed synthetic cell-like objects that move and self-organize in response to self-generated chemical gradients, thereby exhibiting autochemotaxis. Using computational modeling, we specifically focused on microcapsules that encompass a permeable shell and are localized on an adhesive surface in solution. Lacking any internal machinery, these spherical, fluid-filled shells might resemble the earliest protocells. Our microcapsules do, however, encase particles that can diffuse through the outer shell and into the surrounding fluid. The released particles play two important, physically realizable roles: (1) they affect the permeability of neighboring capsules and (2) they generate adhesion gradients on the underlying surface. Due to feedback mechanisms provided by the released particles, the self-generated adhesion gradients, and hydrodynamic interactions, the capsules undergo collective, self-sustained motion and even exhibit antlike tracking behavior. With the introduction of a chemically patterned stripe on the surface, a triad of capsules can be driven to pick up four-capsule cargo, transport this cargo, and drop off this payload at a designated site. We also modeled a system where the released particles give rise to a particular cycle of negative feedback loops (mimicking the "repressilator" network), which regulates the production of chemicals within the capsules and hence their release into the solution. By altering the system parameters, three capsules could be controllably driven to self-organize into a stable, close-packed triad that would either translate as a group or remain stationary. Moreover, the stationary triads could be made to switch off after assembly and thus produce minimal quantities of chemicals. Taken together, our models allow us to design a rich variety of self-propelled structures that achieve complex, cooperative behavior through fundamental physicochemical phenomena. The studies can also shed light on factors that enable individual protocells to communicate and self-assemble into larger communities.

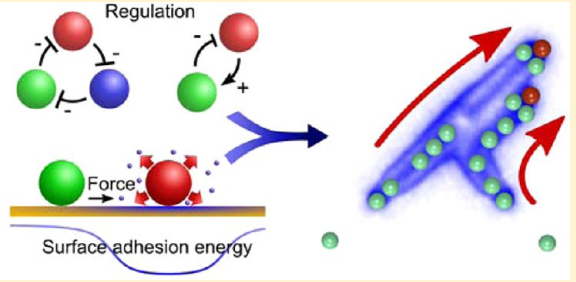

I. INTRODUCTION

One of the critical issues in understanding the origin of life is determining how protocells, the earliest version of living cells, came to communicate with each other and thereby coordinate their actions to achieve greater functionality. In particular, from a fundamental point of view, it is important to establish how protocells developed signaling mechanisms that allowed them to undergo collective motion. The capability to generate signals and sense signals from others, to move in response to these signals, and to assemble into cohesive colonies would have significantly improved the protocells' survivability. Moreover, the ability to distinguish between different entities and selectively organize with one type of species over another would have constituted an important step in the protocells' evolution, enabling their eventual assembly into distinct multicellular entities.

The earliest protocells most likely resembled fluid-filled, self-assembled vesicles.[1] Lacking any complex internal machinery, protocells must have accomplished such vital functions as sensing and communication through basic physicochemical mechanisms, which involved, for example, the diffusion of species through an outer shell. To gain insight into the behavior of early cells, it is potentially useful to examine the survival tactics of primitive organisms such as *Dictyostelium discoideum* (i.e., amoeba or slime mold). The life cycle of *D. discoideum* involves the production and release of chemoattractants that prompt the self-assembly of the individual organisms into large colonies.[2] This mode of communication is referred to as autochemotaxis since the organisms move in response to self-generated chemical gradients. It could be hypothesized that autochemotaxis also enabled communication among protocells.

Inspired by the quest to understand the evolution of the earliest cells, it is intriguing to consider the extent to which simple man-made materials can be made to mimic the interactions among slime molds and amoebas. Namely, can we design synthetic materials that exhibit autochemotaxis? In other words, is it possible to design a material that can generate a signal that is recognized by other similar entities, thereby allowing the entities to move and self-organize into larger structures? The creation of such synthetic systems, which rely on purely physicochemical mechanisms rather than complex biochemical machinery, can provide insight into factors that enabled signaling and cooperative behavior in early cells.

Received: May 20, 2015
Revised: July 27, 2015
Published: July 28, 2015

DOI: 10.1021/acs.langmuir.5b01862
Langmuir 2015, 31, 11951−11963

Another important reason for designing synthetic systems that undergo autochemotaxis is to facilitate the creation of materials that exhibit advanced functionality. Despite the advances in designing active matter and self-propelled particles,[3] there are still few synthetic systems that undergo biomimetic modes of communication, mutually exchanging chemical signals to prompt collective movement.[4−9] The design of synthetic autochemotaxing systems could facilitate the creation of small-scale robotic devices that coordinate their movements and thereby collaborate to perform a concerted function.

The studies presented in this review are motivated by both of these intriguing challenges: (1) to create synthetic materials that are capable of communication that drives collective motion and (2) to gain insight into the factors that enabled signaling and cooperative behavior in early cells. This article is not a comprehensive review of work in this area but rather reflects our recent efforts to address these challenging issues through the development of new computational models. Notably, computer modeling can play a vital role in both the arenas noted above. In particular, while biology offers many powerful design principles, converting these principles into synthetic systems is tremendously challenging without the aid of models that can pinpoint optimal regions in the design space yielding the desired performance or producing totally new, unexpected behavior. In probing the behavior of protocells, computer models can provide a means of testing hypotheses about the conditions of early life that might be difficult to reproduce in the laboratory.

In the studies described in this review, we focus on polymeric microcapsules as our enabling material. We selected these materials for a number of reasons. First, they can be readily synthesized and have been shown to exhibit biomimetic behavior.[10,11] In particular, the capsules have a cell-like structure, with an outer elastic shell enclosing a spherical, fluid-filled domain; moreover, microcapsules are on the same size scale as biological cells. Additionally, microcapsules can encapsulate species within their core and can be driven to controllably release these species through local variations in the environment.[12,13] This is particularly the case for polyelectrolyte microcapsules created by the layer-by-layer (LbL) approach.[11,12] For example, local variations in pH can be harnessed to alter the permeability of the capsule shell and thereby regulate the release of the encapsulated molecules.[12] The released molecules can diffuse in the surrounding solution and act as signaling species, which could trigger responses from neighboring capsules.[14]

We take advantage of the responsive behavior of the capsules' shell to design mobile microcarriers, which are localized on an adhesive surface in solution. The capsules interact through a cycle of bioinspired feedback loops that modulate the release of the signaling species from each of the capsules and give rise to periodic oscillations in the concentrations of these species in the solution.[4,8] As we discuss below, the latter oscillatory behavior has profound consequences when the released species bind to the underlying surface and thereby create adhesion gradients that propel the microcapsules to move. Hence, the coupling of the capsules' communication through the fluid and the substrate enables this system to exhibit autochemotaxis.

While we do not discuss this system here, it is worth mentioning that there is another synthetic system that exhibits oscillatory, self-regulating behavior: self-oscillating gels that are driven to pulsate by the Belousov−Zhabotinsky (BZ) reaction.[15,16] These BZ gels are formed from poly(*N*-isopropylacrylamide) (PNIPAAm) chains that contain grafted ruthenium metal ion catalysts. The BZ reaction produces a periodic reduction and oxidation of Ru, which in turn alters the solvent quality of the polymer. The gel swells when the catalyst is in the oxidized Ru^{3+} state and collapses when the catalyst is in the reduced Ru^{2+} state. Hence, the rhythmic redox reaction produces autonomous swelling and deswelling of the gel so that the sample appears to beat like a heart. In the course of these oscillations, the system produces the activator for the reaction that diffuses from the gel into the surrounding solution. The released activator affects the pulsations of neighboring gel pieces and in turn drives the nearby samples to spontaneously self-aggregate. Thus, this system also displays remarkable forms of autochemotaxis.[7,17,18]

Below, we review our recent computational and theoretical studies on the behavior of the signaling microcapsules that undergo collective motion. As revealed by our findings, these autochemotaxing species can display a remarkably rich dynamic behavior.

II. AUTOCHEMOTAXIS OF SIGNALING MICROCAPSULES

One of the challenges in designing autochemotactic, self-propelled capsules is determining how to exploit the properties of chemical-releasing microcarriers to create interacting, self-regulating systems that exhibit robust, coordinated movement rather than random behavior. To address this challenge, we adapted feedback loops that are ubiquitous in the regulation of biological processes. In our first set of studies, we specifically exploited the coupling between positive and negative feedback that is a hallmark of cellular signaling and thereby designed colonies of microcapsules that could self-organize into various autonomously moving structures and even exhibit antlike tracking behavior.[4] Below, we briefly describe our approach to modeling the behavior of this complex system and discuss the salient findings from our studies.

A. Utilizing Positive and Negative Feedback Loops.

Figure 1 shows the basic components in our simulations: spherical, fluid-filled elastic shells that are immersed in a solution and localized on a substrate. Nanoparticles dissolved in the interior of the capsule can migrate through the capsule's shell and continue to diffuse in the outer solution. Inspired by cellular signaling processes, our 3D simulations encompassed two types of adaptive capsules—signaling and target—which respectively released agonist and antagonist particles into the surrounding fluid. In cellular communication, dissolved agonists bind to the cell and promote the signaling process (production and release of the signal molecule), while antagonists that bind to the cell suppress these processes. In our model, the agonist and antagonist particles performed two important and distinct functions: (1) control the permeabilities of the capsules and (2) alter the capsule−substrate interactions. In particular, the permeabilities of both capsules (and hence the particle release rates) depended on the local concentration of dissolved particles so that the system exhibited a self-regulating mechanism. Additionally, the released particles could adsorb onto the underlying substrate and thereby create adhesion gradients that propelled the microcapsules to move. (The self-imposed adhesion gradients provide an interaction energy that is then converted into kinetic energy as the capsules interact with the surfaces.)

In the simulations, the lattice Boltzmann model (LBM) was used to capture the fluid dynamics of the encapsulated and the external solutions; the LBM is an efficient solver for the Navier−Stokes equation.[19] The lattice spring model (LSM) provides an effective means of simulating the capsule's elastic shell, which is

DOI: 10.1021/acs.langmuir.5b01862
Langmuir 2015, 31, 11951−11963

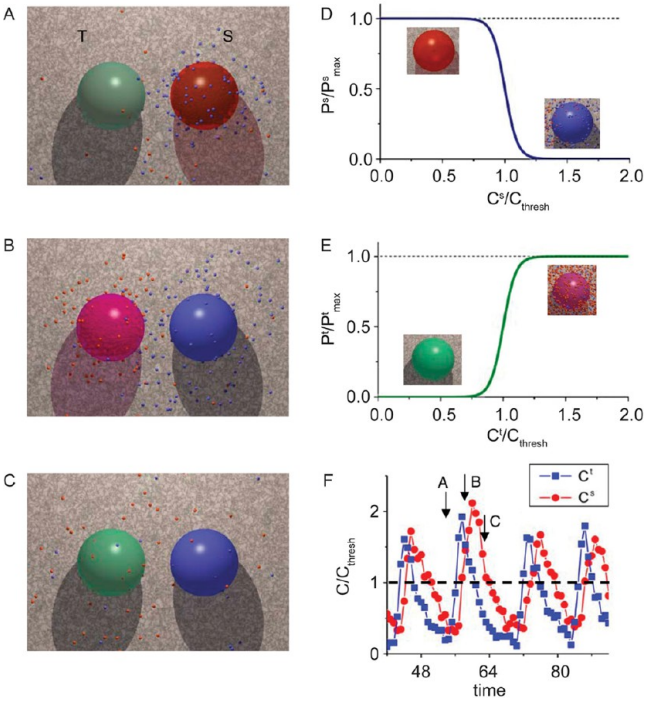

Figure 1. (A–C) Oscillations in the permeabilities of immobilized signaling (right) and target (left) capsules. The color key is shown in (D) and (E). Agonist and antagonist are shown in blue and red, respectively. (D, E) Dependence of P^s and P^t on the respective concentrations of antagonists (C^s) and agonist (C^t) in solution. (F) Periodic oscillations of C^s and C^t near the capsules. Figure adapted from ref 4; reproduced by permission from *Proceedings of the National Academy of Sciences of the United States of America*.

described by a network of harmonic springs that connect regularly spaced masses.[20] The mechanical compliance of the shell can be varied by altering the spring constants for these bonds. Our integrated LBM/LSM approach[21,22] captures the complex fluid–structure interactions in the system, permitting a dynamic interaction between the solid, elastic shell and the surrounding fluid as the moving solid shell exerts a force on the fluid and the fluid, in turn, reacts back on the walls of the shell. In particular, lattice spring (LS) nodes that are situated at the solid–fluid interface impose their velocities on the surrounding fluids; the velocities are transmitted through a linked bounce-back rule to those LBM distribution functions that intersect the moving solid boundary. In turn, LS nodes at the solid–fluid interface experience forces due to the fluid pressure and viscous stresses at that boundary. We calculated the latter force based on the momentum exchange between the LBM particle and solid boundary and then distributed this quantity as a load to the neighboring LS nodes. We validated our 3D LBM/LSM model by determining the drag force on a periodic array of spheres as well as simulating the breathing mode oscillations of a single capsule. In both cases, the simulations showed quantitative agreement with analytical theory.[21]

The signaling capsules release agonists, and the target capsules release antagonists. The released species were modeled as point particles (tracers), which represent nanoparticles or other submicrometer reactants. The particle trajectories obey the following stochastic differential equation:[23] $\mathrm{d}\mathbf{r}(t) = \mathbf{u}(\mathbf{r}, t)\,\mathrm{d}t + (2D_0)^{1/2}\,\mathrm{d}\mathbf{W}(t)$. The first term gives the advection due to the local fluid velocity $\mathbf{u}(\mathbf{r}, t)$. The second term is the Brownian contribution, with D_0 being the particles' diffusion coefficient and $\mathrm{d}\mathbf{W}(t)$ being the differential of a Wiener process with variance $\langle \mathrm{d}W_i\ \mathrm{d}W_j\rangle = \delta_{ij}\mathrm{d}t$, where $i, j = 1, 2, 3$ labels the three spatial coordinates. We neglect backflow effects (i.e., the impact of the particle motion on the flow field) as well as the interactions between the particles.

The permeabilities of the capsules' shells (and hence the particle release rates) depended on the local concentration of the tracer particles in the external solution. To capture the microcapsules' response to the variations in the concentration of agonist, C^t, and antagonist particles, C^s, we model the dependence of the permeability of the capsules' shells in the form of smoothed step functions:

$$P^s = \frac{1}{2}P^s_{max}\left(1 - \tanh\left(\frac{C^s - C_{thresh}}{\Delta C}\right)\right)$$

$$P^t = \frac{1}{2}P^t_{max}\left(1 + \tanh\left(\frac{C^t - C_{thresh}}{\Delta C}\right)\right) \quad (1)$$

Here, P^s_{max} and P^t_{max} are the maximum permeabilities of the signaling and target capsules' shells, respectively. The sharpness of the transition from a dormant state with zero permeability of the capsules' shells to an active state with maximum permeability was taken to be equal to $\Delta C = 0.1 \times C_{thresh}$. We also set the threshold concentration for this transition, C_{thresh}, to be equal for the signaling and target capsules. (As we have reported previously,[4] the value of C_{thresh} plays an important role in the dynamic behavior and structure of the assembled clusters.)

1. Oscillations in Signaling Particles. We first consider the behavior of two capsules that are immobilized on a surface. The above dependence of the permeabilities on C^t and C^s introduces a coupling of positive and negative feedback as illustrated in Figure 1. At the outset of the simulation, the red signaling capsule releases agonist particles, which diffuse in the outer solution. The green target capsules (Figure 1A) also have a permeable shell, which is initially characterized by P^t_{min}. The targets begin to release antagonist (Figure 1E) when the concentration of agonists surrounding these capsules is higher than the threshold value C^t_{thresh}. The released antagonists then diffuse into the solution and thereby affect the signaling capsule. Namely, when the concentration of antagonists around a signaling capsule exceeds a critical threshold C^s_{thresh}, these particles reduce the permeability of the signaling capsule; Figure 1D depicts the dependence of P^s on the local concentration of antagonist. Hence, the signaling capsule releases less agonist. (Here, we set $C^t_{thresh} = C^s_{thresh} \equiv C_{thresh}$.)

At this stage, the low concentration of diffusing agonist causes the target capsule to release fewer antagonists since P^t also depends on the local concentration of agonists (Figure 1E). This small fraction of antagonist eventually diffuses away and has little effect on the signaling capsule. In this manner, this self-regulating system is resets itself so that the signaling capsule again emits a high concentration of agonists and the entire cycle is repeated.

In Figure 1A–C, the color of the capsules indicates the permeability of the shell and serves to emphasize this correlated, dynamic behavior. Importantly, the coupling of the positive and negative feedback loops in this self-regulating system also leads to oscillations in the concentration of agonist and antagonist in the solution (Figure 1F). These oscillations in C^t and C^s prove to be vital to the concerted motion of the capsules. Namely, as noted above, the diffusing agonists and antagonists that adsorb onto the surface alter the capsule–surface interactions; the bound agonists make the surface more adhesive, and antagonists bound

DOI: 10.1021/acs.langmuir.5b01862
Langmuir 2015, 31, 11951–11963

to the surface make the surface less adhesive. Hence, due to the periodic oscillations in these different species, the surface encompasses both sticky and nonsticky areas that affect the movement of the capsules, as described below.

2. Motion of Capsules Due to Self-Generated Adhesion Gradients. To model the response of the capsules to the adhesion gradients generated by the adsorption of the agonists and antagonists onto the underlying surface, we incorporated the capsule−surface interaction via a nonspecific Morse potential, $\phi(r) = \varepsilon_s(1-\exp[-((r - r_0)/\kappa)])^2$, where ε_s and κ characterize the respective strength and range of the interaction potential. The variable r represents the distance between lattice nodes on the capsule's outer surface and the substrate, which is also composed of lattice nodes, and r_0 is the distance where this force equals zero. In our model, diffusing agonists that bind to the surface increase the strength of the capsule−surface interaction, and bound antagonists decrease this quantity. Thus, ε_s is written as $\varepsilon_s = \varepsilon(1 - \theta + \theta')$, where ε is the adhesive strength of the bare surface, θ is the fractional coverage of the surface by the antagonists, and θ' is the corresponding value for the agonists.

The adsorbing species create an adhesion gradient along the surface, and if the gradient is sufficiently asymmetric, then the capsules are driven by enthalpic forces to spontaneously move from a less adhesive to a more adhesive area.[23] An example of this behavior is shown in Figure 2, where the signaling capsule is initially located in the outer layer of a 16-capsule array and $P^t_{max}/P^s_{max} = {}^1/_4$. As the snapshots show, the system self-organizes into a long "snake", with the signaling "head" leading a tail of targets. Notably, the capsules self-organize and move in the absence of an applied stimulus.

Hydrodynamic interactions play a particularly important role in this self-organization because the capsules are moving through a viscous fluid, which mediates their movement. Consequently, the motion of the first few capsules in the solution generates a net force[23] on the neighboring capsules that drives them to follow the moving chain. (Furthermore, the fluid exerts a frictional force that permits the steady motion of the chain.) In fact, if we remove the hydrodynamic interactions in the system (by removing the LBM component of the hybrid simulations), then the motile capsules do not self-organize.

The feedback mechanism is also critical to the observed behavior. If permeabilities P^s and P^t are held constant, then the capsules are seen to scatter in different directions, much like the motion of colliding billiard balls. The disorganized behavior is primarily due to the unchecked deposition of the antagonists, which make the surface less sticky. For the self-adjusting capsules, the agonists diffusing in the solution modulate the amount of antagonist released from the targets.

With a different arrangement of the signaling capsules within a single colony (the 4 × 4 capsule array in Figure 3), the system can form a "dragonlike" structure. Again, the observed collective behavior emerges from viable chemical and physical phenomena, which could be experimentally realized with permeable microcapsules in solution.

With multiple colonies, the capsules can exhibit even more complex behavior, in effect mimicking the behavior of social insects. To generate Figure 4, we applied the following protocol: the colony on the left (C1) is allowed to self-organize while the colony on the right (C2) is held dormant (i.e., localized in space with no particle release) for a fixed number of time steps. At a specified time t_{on}, however, the chemical mechanisms described above are applied to the capsules in C2. As the latter capsules begin to interact, their motion is influenced by the attractive trail of particles left by the first, already mobile cluster. As seen in Figure 4B−D, a triad of C2 capsules turns to follow the trail left by the moving C1 cluster. This behavior indicates that our colonies of synthetic capsules are capable of spontaneously coordinating their actions through the trace of particles left on the surface. It is in this manner that these colonies resemble the behavior of ants, termites and other social insects.

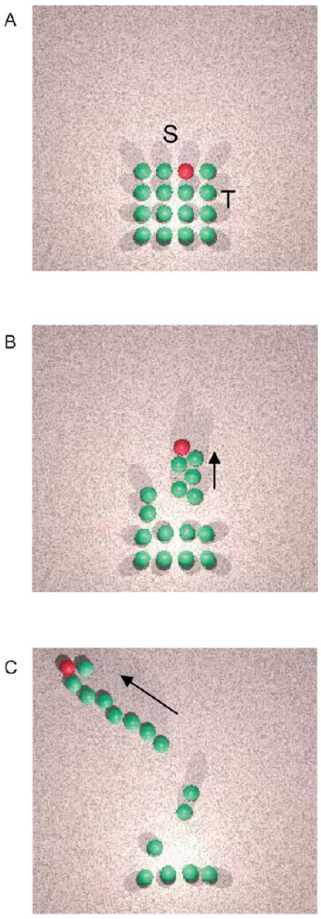

Figure 2. Formation of a mobile snake from an array of self-propelled capsules. The signaling capsule is drawn in red, and the targets are drawn in green. The ratio of the maximum permeabilities of the target and signaling capsules is fixed at $P^t_{max}/P^s_{max} = {}^1/_4$. The size of the simulation box is $L_x \times L_y \times L_z = 200 \times 200 \times 30(\Delta x)^3$, where Δx is the lattice spacing in the lattice Boltzmann model (LBM). The capsule diameter is $10\Delta x$. Hard, stationary walls are positioned at $z = 0$ (the substrate) and $z = 30\Delta x$ (top wall). Periodic boundary conditions are applied along the lateral directions; we used the linked bounce-back boundary conditions at the fluid−wall interface. Figure adapted from ref 4; reproduced by permission from *Proceedings of the National Academy of Sciences of the United States of America*.

We note that in the studies presented above, we focused on the motion of rigid capsules. Given that V is the capsule velocity, μ is the fluid viscosity, and Δx_{LSM} is the lattice space in the LSM, we specifically consider cases where the dimensionless capillary number, $Ca = V\mu/E\Delta x_{LSM}$, is small. Given that E is the Young's modulus and N is the number of capsule nodes in contact with the surface, the capsule−surface interaction strength, $\Phi = \varepsilon N/E\Delta x_{LSM}\kappa^2$, is also taken to be small, and hence the capsules' shapes are close to spherical.[28] In particular, we set the interaction strength of $\Phi = 10^{-2}$ and checked that in simulations $Ca < 10^{-4}$. The same conditions apply to the scenarios considered below, where we considered the behavior of the capsules on chemically patterned surfaces.

DOI: 10.1021/acs.langmuir.5b01862
Langmuir 2015, 31, 11951−11963

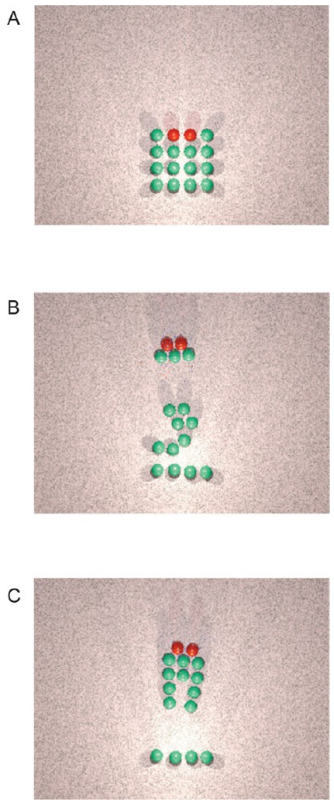

Figure 3. Self-organization of an array with two signaling capsules. The initial setup is shown in (A). A small, mobile cluster (B) forms at C_{thresh} = 7.5, whereas a large two-headed cluster (C) forms at C_{thresh} = 12.5. The nanoparticle concentration is defined in the units of (particles/$(\Delta x)^3$). Here, the threshold concentration of nanoparticles is set equal to $C^t_{thresh} = C^s_{thresh} \equiv C_{thresh}$; the ratio of the maximum permeabilities is $P^t_{max}/P^s_{max} = {}^1/_4$. Figure adapted from ref 4; reproduced by permission from *Proceedings of the National Academy of Sciences of the United States of America*.

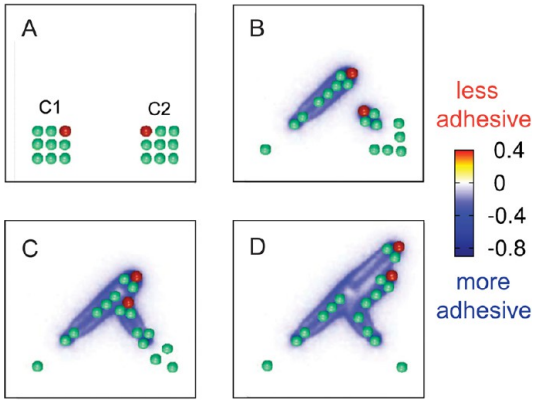

Figure 4. Interaction of two colonies. (A) The initial setup. (B) The colony on the left (C1) starts moving at time t = 0, whereas the colony on the right (C2) is held dormant for t = 500 time steps. (C, D) Eventually C2 capsules follow the trail made by C1 capsules. Parameter $\Delta\theta$ is the difference in the relative concentration of antagonists and agonists on the substrate. The color bar indicates the value of $\Delta\theta$; negative values correspond to more adhesive regions. Figure adapted from ref 4; reproduced by permission from *Proceedings of the National Academy of Sciences of the United States of America*.

3. Pick Up and Drop Off. As noted in the Introduction, the design of synthetic autochemotaxing capsules could facilitate the creation of autonomously operating small-scale devices that perform concerted functions. To demonstrate this functionality, we designed a system of signaling and target microcapsules that pick up, transport, and deliver cargo between locations on an adhesive stripe.[24] In previous studies,[24] we found that one signaling and two target capsules form a particularly stable, self-propelled triad. In particular, this triad moved as a single entity over a range of P^t_{max}/P^s_{max} and C_{thresh} values. Hence, we utilized this combination to form our delivery device (Figure 5). The

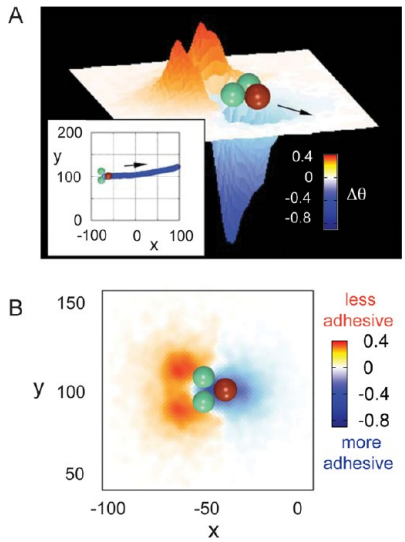

Figure 5. Two different views of the interactions between the triad and a homogeneously adhesive surface ($\varepsilon = 10^{-3}$) computed at t = 300. Time is normalized by the characteristic diffusion time R^2/D_0, where R is the capsule radius and D_0 is the diffusion coefficient of the nanoparticles in solution. Spatial coordinates are measured in lattice Boltzmann units. The parameter $\Delta\theta$ is the difference in the relative concentration of antagonists and agonists on the substrate. The color bar indicates the value of $\Delta\theta$; negative values correspond to more adhesive regions. (A) Adhesive strength $\varepsilon_s = \varepsilon(1 - \theta + \theta')$ is plotted as a topological map, with the peaks corresponding to less adhesive regions and hence barriers to motion; the valleys correspond to more adhesion regions. Inset in (A): trajectory of the triad motion on the homogeneously adhesive surface; the arrow indicates the direction of motion. (B) Top-down view of the triad with the values of $\Delta\theta$ plotted around the capsules. Here, we set $P^t_{max}/P^s_{max} = {}^1/_4$ and C_{thresh} = 12.5. Figure adapted from ref 24; reproduced by permission from The Royal Society of Chemistry (RSC).

inset in Figure 5A (which shows the trajectory of the center of mass of the triad) clearly indicates that the triad undergoes directed motion.

To understand why this triad undergoes such stable self-propelled motion, we carried out simulations on three capsules that were initially placed in an equilateral triangular arrangement on a homogeneous, weakly adhesive substrate and examined the adhesion gradients generated by the released particles. (The initial separation between the centers of the signaling and target capsules was set to 3.5R, where R is the capsule radius.) Figure 5 shows two views of these adhesion gradients; to obtain these plots, we calculated $\Delta\theta = \theta - \theta'$, the difference in the relative concentration of antagonists and agonists on the substrate, and the corresponding value of the adhesive interaction $\varepsilon_s = \varepsilon(1 - \theta + \theta')$ (see above). The agonists emanating from the signaling microcarrier increase the adhesive interaction between the capsules and the substrate; this behavior is indicated by the potential well in Figure 5A and the blue regions in Figure 5B. In

DOI: 10.1021/acs.langmuir.5b01862
Langmuir 2015, 31, 11951−11963

this manner, the adsorbed agonists create an adhesion gradient that effectively pulls the targets to the signaling unit. Thus, the three capsules form a cohesive cluster.

Once the targets come sufficiently close to the signaling capsule, the dissolved agonists can modify the permeability of this target capsule (Figure 1), causing it to release the encapsulated antagonists. The released antagonists that bind to the substrate make this surface less adhesive, as indicated by the bumps in Figure 5A and the yellow regions in Figure 5B. These less adhesive regions prevent the triad from moving backward (i.e., to the left in Figure 5). The latter behavior and the continued release of agonist from the signaling capsule, which creates the more adhesive regions ahead of the triad, drive the capsules to move forward (i.e., to the right) as a coherent unit.

In order to steer the motion of this triad, we introduced a sticky stripe on the surface; this adhesive stripe is drawn in green in Figure 6. Both the signaling and target capsules are more attracted to this stripe than to the rest of the substrate. Moreover, we specified that the signaling capsules are more attracted to the stripe than to the targets. In particular, given that ε_g^t and ε^s are the adhesive strengths for the target and signaling capsules along the green portion of the stripe, we fixed the ratio $\varepsilon_g^t/\varepsilon^s = 2.5 \times 10^{-2}$. Experimentally, the surface of the signaling and target capsules can be functionalized with different types of ligands[25,26] in order to realize this difference in adhesive interactions with the green stripe.

Figure 6A shows the initial configuration of our system; the three capsules on the left constitute our delivery device, or mini-mover, and the cluster of four targets near the stripe constitutes the cargo that must be picked up. At early times ($t = 550$), the two targets and one signaling capsule on the left self-assemble into the stable triad. The triad then moves autonomously along this stripe since this region is more adhesive than the rest of the surface. Thus, the adhesive stripe provides an effective means of regulating the motion of this mini-mover on the surface.

As the triad progresses along the stripe, agonists emanating from the leading signaling capsule adsorb onto the surface and thereby create an adhesion gradient that makes the surface around the four-target cluster more adhesive (Figure 6B,C). Drawn by favorable enthalpic forces, the four targets spontaneously move along the gradient toward the more adhesive region. As the cluster comes in range of the stripe, it ultimately becomes localized on this band due to the relatively strong attractive interactions (Figure 6D). In effect, the triad has deposited a nanoparticle trail that leads the cargo onto the stripe.

Figure 6 also shows that the green stripe contains a blue patch, which permits the drop off and delivery of the cargo at a specific location in the system. In particular, the target capsules experience a weaker adhesive interaction with this blue patch than with the green stripe. In this example, the ratio of the strength of the adhesive interaction for the targets on the blue and green regions is given by $\varepsilon_b^t/\varepsilon_g^t = 0.4$. (The signaling capsules experience the same attractive interaction for both the green and blue regions.) For this value, the green–blue interface forms a sharp adhesion gradient and thus presents a potential barrier for the capsules' motion. Due to this barrier, the four-target cargo is arrested at the green–blue interface. Since the triad contains a leading signaling capsule, the difference between the adhesion strengths of the blue and green regions is not sufficient to stop the mini-mover. As a consequence, the mini-mover passes the blue region and continues its movement along the stripe (Figure 6E).

Clearly, there is an optimal range of adhesion strengths for which the triad can perform as an autonomous pick-up and

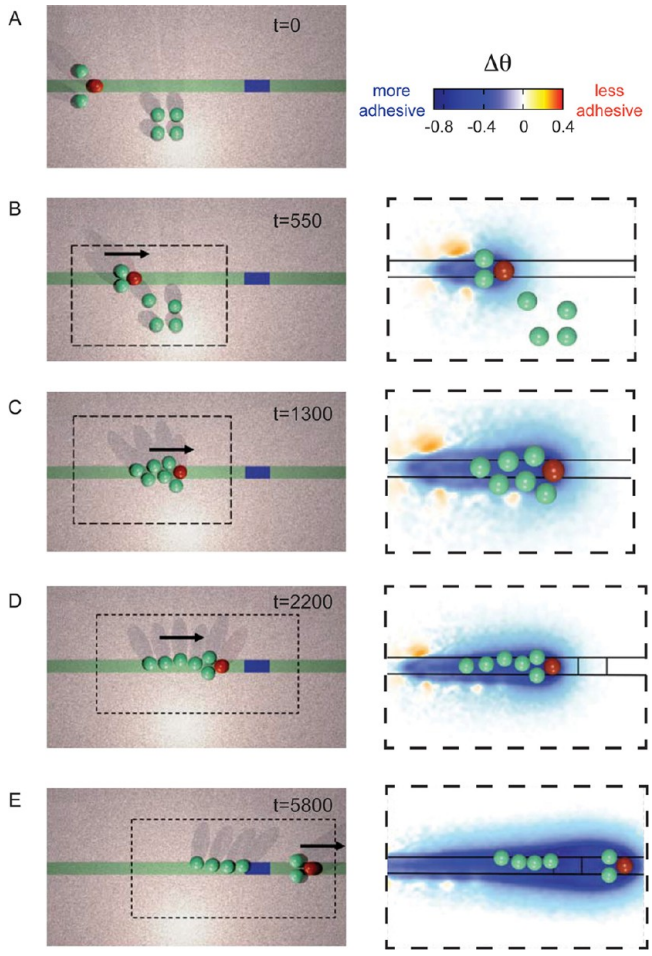

Figure 6. Left column: (A–D) Top-down view of the formation and motion of a mobile train along the green adhesive stripe; the blue patch represents the less adhesive region. (E) The four-capsule cargo is arrested at the blue patch on the stripe while the triad continues to move. Right column: changes in the adhesion strength on the surface in the regions marked by the dotted lines in the left frames. The blue patch is positioned at $x_1 = 60\Delta x$. The ratio of the adhesive strengths for the target and signaling capsules in the green portion of the stripe is set equal to $\varepsilon_g^t/\varepsilon_s = 2.5 \times 10^{-2}$; the same ratio at the blue patch is $\varepsilon_b^t/\varepsilon_s = 10^{-2}$. Other parameters in the simulations are the same as in Figure 5. Figure adapted from ref 24; reproduced by permission from The Royal Society of Chemistry (RSC).

delivery device. In the simulations,[24] we generated a phase map to pinpoint this range by systematically varying the strengths of adhesion between the target capsules and the green and blue stripes (ε_g^t and ε_b^t, respectively). We observed that for relatively low values of ε_g^t and ε_b^t, the triad can pick up and drop off the cargo. Namely, after the successful pick up and as the train (triad and cargo) approaches the blue patch, the four-target cargo remains localized at this location; the triad, however, keeps moving along the path, as shown in Figure 6E. At higher adhesions strengths, however, the entire train reaches the blue patch and stops, with the signaling bead being localized on the blue patch. When $\varepsilon_g^t = \varepsilon_b^t$, the strengths of adhesion to the blue and green paths are equal; therefore, the adhesion gradient at the green–blue interface is zero and the entire train passes the blue part and keeps moving along the stripe. At high adhesion along the stripe, the train eventually stops at an intermediate position, without reaching the blue patch. This phase map delineates the values of ε_g^t and ε_b^t that lead to the effective pick up, transport, and drop off of the target cargo.

DOI: 10.1021/acs.langmuir.5b01862
Langmuir 2015, 31, 11951–11963

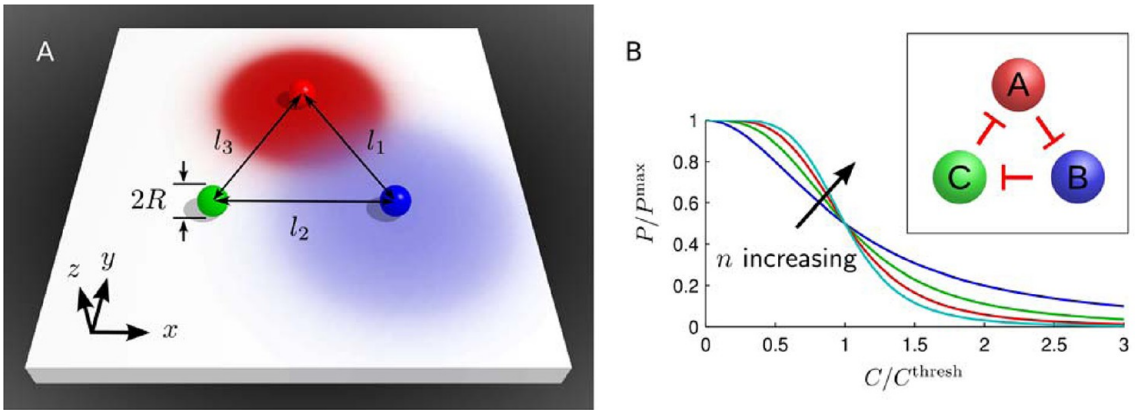

Figure 7. System of three microcapsules on a surface and production-regulating repressilator feedback network. (A) Snapshot of a simulation with colored regions around capsules indicating the density of chemicals adsorbed onto the substrate. The capsule diameter is $2R = 7\Delta x$ where $\Delta x \approx 1$ μm is the lattice Boltzmann grid spacing. The simulation domain is of size $42R \times 42R \times 4R$ and is periodic in the x and y directions with no-slip z boundaries. (B) Curves of the chemical production rate as functions of the local repressor concentration C, modeled by the Hill function with values of the Hill coefficient of $n = 2$, 3, 4, and 5. (Inset) Schematic of the repressilator network: capsule A produces a repressor of B, capsule B produces a repressor of C, and capsule C produces repressor of A. Figure from ref 8; reproduced by permission from The Royal Society of Chemistry (RSC).

Once the triad has deposited its cargo, it can potentially move along the track created by the stripe to pick up a new payload; additional blue patches would enable this second load to be deposited further down the line. Thus, this system could provide an effective means of autonomously transporting a broad range of particulates (and the encapsulated substances) within microfluidic devices. Notably, the cooperative behavior exhibited by the capsules is driven simply by the self-generated gradients in the presence of the chemically patterned stripe, which is the only externally imposed stimulus in this system.

B. Harnessing a Cycle of Negative Feedback Loops. The above studies relied on the coupling of positive and negative feedback loops. We subsequently implemented another form of biomimetic feedback into our system to test the generality of our findings that self-generated and self-regulating signals can drive the self-organization and collective motion of the synthetic capsules. In particular, we adapted the negative feedback loop exemplified by the repressilator network.[27] In the original study,[27] the repressilator involved three genes that were coupled through negative feedback so that each gene repressed the following gene in the loop and was repressed by the previous one in the cycle. The repressilator was specifically designed to produce oscillatory dynamic behavior and thereby introduce temporal oscillations into a living cell. In our recent work,[8] we imposed the repressilator network on a group of three microcapsules, as shown in Figure 7. The capsules, labeled A, B, and C, respectively generate and release chemicals a, b, and c. The presence of chemical a reduces the activity of microcapsule B; likewise, b suppresses microcapsule C, and c suppresses microcapsule A. The capsules are localized on a substrate, and the entire system is immersed in a host fluid.

In our simulations,[8] we model each capsule in Figure 7 by a Lagrangian mesh of nodes, with elastic bonds connecting neighboring pairs of these nodes. As in section IIA, flow field $\mathbf{u}(\mathbf{x}, t)$ is solved numerically using the lattice Boltzmann method.[28,29] The immersed boundary method (IBM) is used to efficiently couple the dynamics of the capsules to the fluid flow.[30,31] Mesh nodes of the capsule are advected with the local fluid flow, and the elastic deformation of the mesh results in restoring forces which act on the fluid to drive flows. The latter processes allow the deformations to relax while approximately satisfying no-slip conditions on the mesh nodes. No-slip boundary conditions are also imposed on the top and bottom walls via lattice Boltzmann bounce-back rules, and periodic conditions are used for the lateral domain boundaries.

While previous studies have revealed oscillatory dynamics in the well-mixed repressilator system,[27,33] to the best of our knowledge, our study[8] was the first to model the behavior in a system where the constituent components are produced in spatially separated locations. As we discuss below, imposing the repressilator network on chemical-releasing microcapsules can also lead to oscillatory chemical behavior, which then allows the microcapsules to move autonomously and exhibit self-regulating self-organization. In the study, we also describe how the range of interactions between the capsules can be tuned so that capsules can effectively sense each other and aggregate from relatively large initial separations (over 10 microcapsule radii).

1. Chemical Oscillations from Immobile Source Capsules. To understand and predict the possible outcomes of our microcapsule system, we first analyzed a specific, simplified scenario where the three capsules are immobile and fixed in an equilateral triangular configuration on the substrate (Figure 7A). We developed a theoretical model and performed a linear stability analysis to pinpoint the regions in phase space that yielded oscillatory production rates in all of the chemical species.

Within our theoretical model, the concentrations of the three chemicals are denoted as C_j, $j = 1, 2, 3$. Capsule j is located at point $\mathbf{X}_j$ and produces chemical j at a rate P_j. As illustrated schematically in Figure 7B, the production of chemical j (by capsule j) depends on the concentration of chemical $(j - 1)$ (modulo 3) at capsule j. As in previous models of repressilator systems,[27,33] we use the Hill function[32] to model the inhibitory action of the repressor species, with concentrations C_{j-1}, on the rates of production P_j of the chemicals. Applying the Hill function to our microcapsules gives production rates of the form

$$P_j = \frac{P^{\max}}{1 + \left(\frac{C_{j-1}(\mathbf{X}_j)}{C^{\text{thresh}}}\right)^n} \tag{2}$$

where $P^{\max}$ is the maximum, unrepressed production rate and C^{thresh} is the threshold repressor concentration at which production crosses over from high to low levels. The Hill

DOI: 10.1021/acs.langmuir.5b01862
Langmuir 2015, 31, 11951−11963

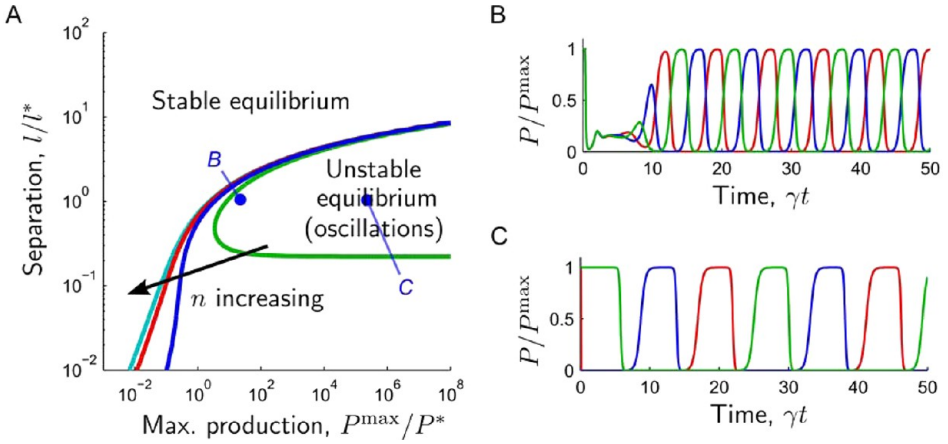

Figure 8. (A) Phase diagram for the stability of the equilibrium point based on the immobile repressilator system with equal distances between each pair of capsules. For each point in parameter space and a given choice of Hill coefficient n, there is a steady state that is stable for parameters on the left of the respective curve and unstable on the right. Points labeled B and C indicate parameter values used in (B) and (C) respectively. (B, C) Examples of time series for production rates of the three chemical components: a (red), b (blue), and c (green) in the oscillatory regime with $n = 3$. Figure adapted from ref 8; reproduced by permission from The Royal Society of Chemistry (RSC).

coefficient, n, in the Hill function controls the steepness of the transition (Figure 7B).

The concentration fields are governed by the reaction−diffusion equation,

$$\partial_t C_j = D\nabla^2 C_j - \gamma C_j + P_j \delta(\mathbf{X}_j) \tag{3}$$

where D is the diffusivity and γ is the first-order decay constant; both parameters are assumed to take the same value for all chemical species. The symbol δ denotes the Dirac delta function, representing a point source for each chemical at the respective capsule position. Chemical advection with fluid flow was not considered in the analysis involving immobile capsules. To simplify the analytical expressions, we considered the capsules to lie on the no-flux plane boundary of a half-space domain. This neglects other boundaries present in the finite computational domain used in the simulations, but the discrepancy is expected to be negligible for large-enough domains.

To describe the behavior of the system in nondimensional parameters, we identified the characteristic length scale as $l^* = (4D/\gamma)^{1/2}$, which quantifies the diffusive range of the chemical before it is degraded, and the production scale as $P^* = \pi^{3/2} l^{*3} \gamma C^{\text{thresh}}/2$. We found that the system always displays a unique steady state in which all capsules have equal, constant production rates. (The symmetry is due to considering only the special case with all intercapsule distances equal to the same value, l.) The stability of this steady state depends on three dimensionless parameters: n, $P^{\max}/P^*$, and l/l^*. Specifically, for fixed n and l/l^*, the steady state is unstable if $P^{\max}/P^* > P^{\text{crit}}$ and stable otherwise. The critical production rate P^{crit} can be defined as

$$P^{\text{crit}}(n, l/l^*) = \begin{cases} \dfrac{1}{\sqrt{\pi}} \exp\left(\dfrac{2l}{l^*}\right) \dfrac{1}{1-\zeta} \left(\dfrac{\zeta}{1-\zeta}\right)^{1/n}, & \text{if } \zeta < 1 \\ \infty, & \text{otherwise} \end{cases} \tag{4}$$

where $\zeta(n, l/l^*) = (1/n) \exp({}^1/_3(\pi^2 + 4(l/l^*)^2)^{1/2} - 2l/l^*)$.

The boundaries between stable and unstable equilibria, given by P^{crit}, are plotted in Figure 8A. Importantly, the equilibrium state is always stable if $n = 1$ as the condition $\zeta < 1$ is not satisfied by any capsule separation l/l^*. In the case of $n = 2$, it is possible to achieve an unstable steady state but only if $l/l^* > l^{\min} \approx 0.22$. For $n \geq 3$, P^{crit} is finite for any value of l/l^*, so the steady state can always be made unstable by choosing $P^{\max}$ to be sufficiently large. The curves of P^{crit} converge as n increases beyond $n = 3$. The behavior of the system is therefore qualitatively sensitive to the value of the Hill coefficient if n is small, but large values of n give rise to the same behavior.

We note that in the equivalent well-mixed system (without spatial heterogeneity), it is known that the $n = 2$ case does not permit sustained oscillatory solutions.[33] Hence, the time lag introduced by diffusive communication appears to destabilize the steady state. The cutoff distance $l^{\min}$ roughly characterizes the capsule separation beyond which the diffusive delay becomes important and below which the system behaves as if it were well mixed.

To validate our findings from these analytical calculations, we performed simulations of immobile microcapsules with repressilator-controlled chemical production rates. These simulations employed a finite difference method to evolve the chemical concentration fields. Good agreement was found between theory and simulations, with large-amplitude oscillations developing when the steady state was unstable. Figure 8B,C exemplifies the oscillatory dynamics of the production rates in the unstable regime. The three capsules cyclically switch on and off. In Figure 8B, the parameters are close to the critical boundary between steady and oscillatory regimes. Moving further away from the boundary by increasing the maximum production rate yields longer periods of oscillation and more distinct separation between the decline in the production of one chemical and the rise in the production of the next (Figure 8C).

2. Microcapsule Aggregation. Having ascertained parameter regimes that respectively yield steady and oscillatory chemical dynamics, we proceeded to analyze the motion of the microcapsules driven by this chemical activity. In particular, we considered that chemicals a, b, and c could adsorb onto the surface under the capsules and subsequently modify the adhesive interactions between the capsules and the surface. As explained in section IIA, gradients in the interaction strength generate enthalpic forces that propel the capsules along the surface.

To model the adsorption process, we imposed partially adsorbing boundary conditions[34] for the three chemical fields on the lower surface $z = 0$,

$$D\partial_z C_j|_{z=0} = K(1-\theta) C_j|_{z=0} = f_j^{\text{ads}} \tag{5}$$

DOI: 10.1021/acs.langmuir.5b01862
Langmuir 2015, 31, 11951−11963

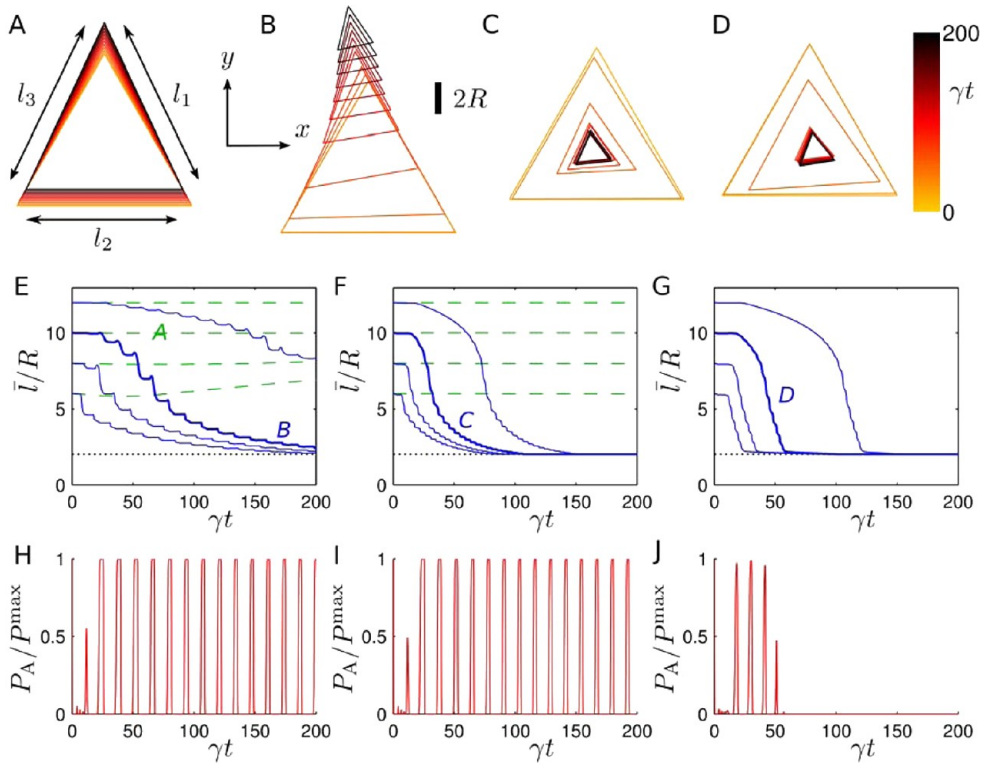

Figure 9. Self-induced motion of three capsules under different conditions. (A–D) Examples of capsule migration on a substrate. The configurations of the three capsules are plotted as triangles representing the center-to-center vectors between capsules at regular time intervals. The color of each triangle indicates the time, as shown in the color bar. A scale bar indicates the diameter of the capsules, $2R$. (A) Constant production rates; only a increases the surface adhesion. (B) Oscillatory repressilator kinetics with $n = 3$; only a increases the surface adhesion. (C) Oscillatory repressilator kinetics with $n = 3$; all chemicals increase the surface adhesion. (D) The same as in (C) with $n = 2$. (E) Average distance between capsules as functions of time if only chemical a increases the surface adhesion. Solid curves show results for capsules controlled by repressilator kinetics ($n = 3$) starting with four different separation distances, and dashed curves correspond to constant production rates for all capsules. Labeled curves correspond to the simulations shown in the subfigure with the same label. (F) The same as in (E) with all adsorbed chemicals increasing the surface adhesion. (G) The same as in (F) with Hill coefficient $n = 2$. (H–J) Oscillations in the production of chemical a for the simulations shown in (B–D), respectively, and in bold in (E–G), respectively. Figure from ref 8; reproduced by permission from The Royal Society of Chemistry (RSC).

where K is the maximum adsorption rate and $\theta(x, y, t) = (\theta_1 + \theta_2 + \theta_3)$ is the local surface coverage fraction. We assume that there is a finite capacity for the surface to hold adsorbed species, and hence the distribution of adsorbed chemicals is nonlinear with chemical production rates. Importantly, the adsorption capacity is shared by all chemical species, so there is an effect of competition between species. Also, since the chemicals degrade over time, saturation of the surface is not irreversible but evolves dynamically as the local concentrations of the three species in the fluid change. Further details of boundary conditions and the evolution of the surface coverage field θ are given in ref 8.

Generalizing the capsule–surface interaction energy introduced in section IIA, we write $\varepsilon_s = \varepsilon + \sum_j(\beta_j\theta_j)$, where β_j represents positive (for repulsion) or negative (for attraction) coefficients for the contributions from each adsorbed species θ_j. A capsule on the surface experiences a lateral driving force due to the surface gradient in interaction energy $\mathbf{F}^{adh} = -\eta\nabla_{\|}\varepsilon_s = -\eta\sum_j(\beta_j\nabla_{\|}\theta_j)$, where $\nabla_{\|}$ denotes the gradient operator applied only in the x and y- directions (parallel to the wall). In our study, we specifically considered two scenarios with different combinations of β_j. For scenario I, we set $\beta_1 < 0$ and $\beta_2 = \beta_3 = 0$. Hence, chemical a increases the adhesion between the capsules and the surface while b and c adsorb onto the surface without affecting capsule–surface interactions. In scenario II, we assume that all species equally contribute attractive interactions, $\beta_1 = \beta_2 = \beta_3 < 0$.

We focus on cases where the Peclet number (Pe) in our systems is relatively low, $Pe = UR/D < 0.5$ (where U is the capsule speed induced by the adhesion gradients). As a result, chemical transport is dominated by diffusion, and our previous theoretical results for immobile capsules can be applied to help understand the behavior in the system of moving capsules. The motion is also characterized by low Reynolds numbers, $Re = UR/\nu < 0.01$, so inertial effects are not important (here ν is the fluid kinematic viscosity).

Recall that our aim was to isolate scenarios where the self-regulating capsules underwent autochemotaxis; namely, we attempted to pinpoint parameters where the release of chemicals from the different capsules led to their self-organization and subsequent directed motion. We found that oscillations in the production of the released species (a, b, and c) were crucial to achieving this form of collective behavior. This observation is evident in Figure 9A–D, which shows the temporal behavior of the three capsules in the presence and absence of the repressilator scheme (for cases I and II). (Note that the absence of the repressilator feedback means that there is a constant production of a, b, and c.)

Figure 9A shows the case in which the self-regulation is removed (thus yielding constant production rates), and it is only the adsorbed a species that increases the surface adhesion. As can be seen, there is little net motion of capsules (even over relatively long time scales). The lack of motion is due to the fact that the

DOI: 10.1021/acs.langmuir.5b01862
Langmuir 2015, 31, 11951–11963

surface under each capsule is essentially saturated with the respective capsule's product. The slight gradients in a pull B and C slowly toward A, but they also repel capsule A from B and C.

The situation is, however, quite different when we implement the repressilator dynamics (with $n = 3$) and thus introduce self-regulation into the system. For scenario I (where surface adhesion is increased only by adsorbed a), the capsules now rapidly self-organize into a single triad, which acts as a cohesive unit as it continues to migrate (Figure 9B). Because the capsules are now self-regulating, they effectively take turns producing (and releasing) their respective products. Hence, when the level of a is high, the levels of b and c in the system are relatively low. Consequently, capsules B and C experience large gradients in a and are strongly attracted toward capsule A. (To optimize this collective behavior, a large maximum production rate of $P^{max}/P^* = 3 \times 10^5$ is used.)

Under scenario II, all species increase the surface adhesion when adsorbed on the surface. The behavior is similar to that in scenario I, but now all three capsules become attractive when active. This results in more rapid aggregation of the capsules, but the lack of asymmetry means that the assembled triad does not migrate in any direction (Figure 9C). We also examined this scenario with Hill coefficient $n = 2$ instead of $n = 3$ and found the same self-assembling behavior to emerge.

To show that these capsule dynamics are robust, we repeated the simulations with a range of initial separations between capsules. Plots of the average capsule separations for the two scenarios are given in Figure 9E–G. Constant production rates (dashed curves in Figure 9E,F) consistently failed to produce capsule aggregation since surface saturation prevented the formation of adhesion gradients under the capsules.

When production rates were modulated by repressilator-induced oscillations, however, the microcapsules could readily aggregate (solid curves in Figure 9E–G). As expected, if all chemicals increase the surface adhesion (scenario II, Figure 9F), then aggregation is significantly faster than if only one chemical drives the motion (scenario I, Figure 9E).

Although aggregation was observed for both Hill coefficients $n = 2$ and 3, important differences between the two cases should be noted. First, under the $n = 3$ condition, the rate of aggregation decreases as the capsules approach each other, while this slowing down is not seen when $n = 2$. Second, the amplitude of chemical production oscillations is relatively insensitive to capsule separation when $n = 3$ (Figure 9H,I), while production drops to negligible values once the capsules have aggregated with $n = 2$ (Figure 9J). These two features are, in fact, related. The decay in oscillations in the $n = 2$ case is explained by our theoretical analysis, which predicted that oscillations cannot be sustained when the capsules are too close together. As the capsules aggregate, the chemical oscillations are reduced in amplitude, saturating a smaller and smaller region of the surface and thereby maintaining large adhesion gradients in the vicinity of the three approaching capsules. Eventually, the oscillations cease completely and the capsules mutually repress each other with a low, constant production. In contrast, with $n = 3$, oscillations persist even at small separations. Figure 9H,I shows that the quasi-periodic chemical production profile does not change much as the capsules aggregate. The released chemicals continue to saturate a large area, encompassing all three capsules, when the production rates peak so that the adhesion gradients felt by the capsules become smaller as their separation decreases.

Although the final configuration of the capsules, a close-packed triad, is the same in the $n = 2$ and 3 cases, we have shown that their chemical behavior can be qualitatively different. With $n = 3$, oscillatory chemical production remains high after aggregation, so the capsules continue to be chemically active and could migrate collectively (if there is asymmetry in β_j values) while potentially attracting other particles through the generated surface adhesion gradients. In the $n = 2$ system, the capsules become effectively inactive once aggregation is complete, resulting in a more self-contained, single-purpose aggregation process.

III. CONCLUSIONS

In these computational studies, we simulated the behavior of microcapsules that were localized on an adhesive surface and encapsulated signaling particles, which could diffuse from a capsule's inner core and into the outer solution. Polymeric microcapsules can readily be fabricated to be the same size as biological cells; moreover, the outer shells of these capsules can be highly reactive to environmental changes and thus exhibit a biomimetic response to external stimuli. Using our models for these cell-like objects, we imposed a set of bioinspired feedback loops onto this system. These feedback loops enabled the system to exhibit self-regulation, which in turn led to pronounced oscillations in the concentrations of signaling particles in the solution. Because these particles could also bind to the surface underneath the capsules and modify the capsule–surface adhesion strength, the oscillatory behavior was vital to generating gradients in interaction energies that prompted the microcapsules to undergo collective motion. To summarize, we designed a physically realizable self-regulating system of microcapsules which reacted to self-produced chemical signals by undergoing directed motion and self-assembly.

In the system involving the coupling of positive and negative feedback loops, the individual capsules could self-organize into long, self-propelled trains. With distinct colonies of capsules, the system could display tracking behavior analogous to that performed by ants and termites. In particular, capsules from one group could follow the chemical trail left by capsules from another mobile group. We exploited this behavior to design a stable trio of capsules that could pick up and drop off cargo, guided by a chemically patterned patch on the surface.

We also examined the effect of imposing cycle of negative feedback loops onto the system that were inspired by the biomimetic repressilator dynamics. As in the system described above, the capsules displayed oscillations in the production of their respective species. These chemical oscillations were again vital in driving the self-organization of the capsules. Namely, in the absence of oscillations in a, b, and c, the surface became saturated with these molecules and did not exhibit the gradients in adhesion necessary to propel the capsules. By imposing self-regulation via the cycle of negative feedback, some capsules were temporarily inactive and thus could feel the adhesion gradients generated by the neighboring active capsules. Moreover, we found that capsules separated by as much as 10 radii could aggregate into a cohesive group due to these self-generated surface gradients.

In the repressilator-inspired system, we examined cases where either just one or all of adsorbed species affected the surface adhesion and thereby demonstrated a means of driving the microcapsules to self-organize into either mobile or stationary triads. We also pinpointed parameters that caused the rapidly assembling microcapsules to then become dormant and thus produce just minimal quantities of any chemical. These findings indicate that the functionality of the responsive capsules can be

DOI: 10.1021/acs.langmuir.5b01862
Langmuir 2015, 31, 11951–11963

tailored for specific applications; for instance, the mobile triads can be harnessed in microfluidic devices for the self-sustained transport of particulates. On the other hand, the triads that become stationary once they have assembled can form a fundamental building block in the bottom-up assembly of larger, stationary structures.

Such studies on simple cell-like capsules shed light on potential physicochemical factors that facilitate interactions between protocells. Given that the predecessors of modern cells lacked complex biochemical machinery, intercellular communication and coordinated behavior are likely to have been based on relatively simple processes, such as the diffusion of chemoattractants or other molecules through a porous membrane. Our studies demonstrate examples in which temporal oscillations in released chemoattractants, governed by simple chemical interaction networks, could result in aggregation into clusters and collective motion. It is interesting that the autochemotactic aggregation of slime molds also involves coordinated pulses of chemoattractant released by the individuals.[35] This is particularly notable because the collective motion of primitive unicellular organisms can yield insight into the emergence of cooperative behavior in protocells.

Our model also allows us to formulate design principles for producing a rich variety of artificial cells capable of undergoing self-sustained, cooperative behavior. (Notably, we have also modeled three-dimensional compliant capsules that exhibit more ellipsoidal shapes and thus might more closely resemble the flexibility of biological cells.[36]) These systems do not need an external input or additional energy source to drive their motion and collective behavior. Hence, our findings could guide the development of smart micromachines or microrobots that can be made to perform without an external energy supply. Our computational model also provides a new approach to simulating cell-signaling processes and can yield greater insight into the interrelationships among the signaling events, the movement of compliant cells, and hydrodynamic interactions.

Finally, we note that there are a number of experimental studies indicating that many of the necessary components are in place to create the active assemblies described above (discussions in refs 8 and 24). For example, a salient feature of the capsules described in section II.A is a coupling of positive and negative feedback that gives rise to the self-regulation of the capsules' permeability. Notably, there is a vital application where LbL microcapsules exhibit analogous behavior, modulating the shells' permeability via feedback loops. In this scenario, the capsules contain corrosion inhibitors and are embedded in a film.[12] When the corrosion process occurs in the film, it releases byproducts that alter the local pH. The permeability of the polyelectrolyte shells strongly depends on pH, and when the pH is changed in the neighboring area, the shells' permeability increases to release the corrosion inhibitor. The released inhibitor suppresses the corrosion, and the original pH value is restored, causing the shells' permeability to decrease. The responsiveness of the LbL capsules to local variations in the environment and the subsequent triggered released of the encapsulated species make these microcarriers ideal materials for realizing our predictions.

There is also experimental evidence[37,38] that nanoparticles released from mobile microcapsules would be effective at regulating the capsules' motion on the underlying surface. In particular, a small fraction of adsorbed "sticky" nanoparticles were found to be highly effective at retarding and even arresting the fluid-driven motion of the colloids over the surface.[36] In other words, these particles would make the surface more sticky for the capsules, achieving a function of the agonists described above.

Another set of experiments[39] suggests a means of utilizing released nanoparticles to make the surface less sticky for the microcapsules and thus promote the capsules' motion on this substrate (i.e., realize the role of the antagonist in our system). Specifically, the substrate could be coated with ligands that are attracted to functional groups distributed sparsely on the surface of the microcapsules or polymersomes.[39] The encapsulated nanoparticles would encompass a higher surface coverage of the same functional groups. Consequently, when these nanoparticles were released and diffused near the substrate, the ligands would preferentially bind to the more functionalized (i.e., more attractive) nanoparticles and release their hold on the loosely bound microcapsules.

We also point to our computational simulations[40] and subsequent experimental studies[41] demonstrating that fluid-driven, nanoparticle-containing microcapsules can recognize variations in surface energy and respond to these variations by controllably releasing the encapsulated cargo. Taken all together, these experiments[12,37−39,41] indicate the feasibility of fabricating responsive microcapsules that controllably release nanoparticles to create adhesion gradients, which in turn direct their motion. Thus, we can move closer to creating self-propelled microcarriers which can leave a trail of nanoparticles that is sensed by nearby units, thereby forming a biomimetic, autochemotaxing colony.

AUTHOR INFORMATION

Corresponding Author

*E-mail: balazs@pitt.edu.

Notes

The authors declare no competing financial interest.

Biographies

Victor V. Yashin obtained his Ph.D. in physics from M. V. Lomonosov Moscow State University in Moscow, Russia in 1989 under the supervision of Dr. Alexander S. Mikhailov. From 1987 to 1996, he worked at the Institute of Petrochemical Synthesis of the Russian Academy of Sciences, where he developed a theory for macromolecular reactions in polymer blends. In 1996, Victor moved to the University of Akron to work on modeling the ultrasonic degradation of rubbers. In 2003, Victor joined Dr. Anna C. Balazs's group at University of Pittsburgh and is now a visiting research assistant professor. His current research interests are in modeling responsive and active soft materials.

DOI: 10.1021/acs.langmuir.5b01862
Langmuir 2015, 31, 11951−11963

German V. Kolmakov is an assistant professor of physics at the NYC College of Technology, the City University of New York. After his education at the Moscow Institute of Physics and Technology (MIPT) and L. D. Landau Institute for Theoretical Physics, he worked at the Institute of Solid State Physics, Lancaster University, and the University of Pittsburgh. His research interests include condensed matter physics and nonlinear dynamics.

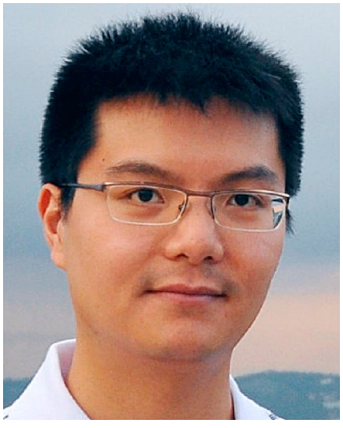

Henry Shum received his M.Math.Phys. degree from the University of Warwick and completed his D.Phil. in mathematical sciences at the University of Oxford. He held a postdoctoral position at the Rudolf Peierls Centre for Theoretical Physics at the University of Oxford before moving to the University of Pittsburgh, where he is currently a postdoctoral scholar. His research interests involve the modeling and simulation of microscale systems, including microorganism motility, active self-assembly, and electrokinetic phenomena.

Anna C. Balazs is a distinguished professor of chemical engineering and the Robert von der Luft Professor at the University of Pittsburgh. She received her B.A. in physics from Bryn Mawr College and her Ph.D. in materials science from the Massachusetts Institute of Technology. After postdoctoral work in the Polymer Science Department at the University of Massachusetts, Amherst, she joined the faculty at the University of Pittsburgh. Her research involves developing theoretical and computational models to capture the behavior of polymeric materials, nanocomposites, and multicomponent fluids. Balazs is a Fellow of the American Physical Society, the Royal Society of Chemistry, and the Materials Research Society. She received the American Chemical Society Langmuir Lecture Award in 2014. In 2015, she received the Royal Society of Chemistry S F Boys-A Rahman Award.

■ ACKNOWLEDGMENTS

A.C.B. acknowledges financial support from the DOE Biomaterials Program and DOE EFRC centered at Northwestern University.

■ REFERENCES

(1) Chen, I. A.; Walde, P. From self-assembled vesicles to protocells. *Cold Spring Harbor Perspect. Biol.* **2010**, *2*, a002170.
(2) King, J. S.; Insall, R. H. Chemotaxis: Finding the Way Forward with Dictyostelium. *Trends Cell Biol.* **2009**, *19*, 523−530.
(3) Ebbens, S. J.; Howse, J. R. In Pursuit of Propulsion at the Nanoscale. *Soft Matter* **2010**, *6*, 726−738.
(4) Kolmakov, G. V.; Yashin, V. V.; Levitan, S. P.; Balazs, A. C. Designing Communicating Colonies of Biomimetic Microcapsules. *Proc. Natl. Acad. Sci. U. S. A.* **2010**, *107*, 12417−12422.
(5) Bhattacharya, A.; Balazs, A. C. Biomimetic Chemical Signaling Across Synthetic Microcapsule Arrays. *J. Mater. Chem.* **2010**, *20*, 10384−10396.
(6) Bhattacharya, A.; Balazs, A. C. Designing Microcapsule Arrays That Propagate Chemical Signals. *Phys. Rev. E* **2010**, *82*, 021801.
(7) Dayal, P.; Kuksenok, O.; Balazs, A. C. Reconfigurable Assemblies of Active, Autochemotactic Gels. *Proc. Natl. Acad. Sci. U. S. A.* **2013**, *110*, 431−436.
(8) Shum, H.; Yashin, V. V.; Balazs, A. C. Self-assembly of Microcapsules Regulated via the Repressilator Signaling Network. *Soft Matter* **2015**, *11*, 3542−3549.
(9) Sen, A.; Ibele, M.; Hong, Y.; Velegol, D. Chemo and Phototactic Nano/microbots. *Faraday Discuss.* **2009**, *143*, 15−27.
(10) Stadler, B.; Price, A. D.; Chandrawati, R.; Hosta-Rigau, L.; Zelikin, A. N.; Caruso, F. Polymer Hydrogel Capsules: En Route Toward Synthetic Cellular Systems. *Nanoscale* **2009**, *1*, 68−73.
(11) Sukhorukov, G. B.; Mohwald, H. Polyelectrolyte Microcapsules as Biomimetic Models. In *Colloids and Colloid Assemblies*; Caruso, F., Ed.; Wiley-VCH, 2003; Chapter 18, pp 561−580.
(12) Shchukin, D. G.; Zheludkevich, M.; Yasakau, K.; Lamaka, S.; Ferreira, M. G. S.; Mohwald, H. Layer-by-Layer Assembled Nanocontainers for Self-Healing Corrosion Protection. *Adv. Mater.* **2006**, *18*, 1672−1678.
(13) Kempe, K.; Noi, K. F.; Ng, S. L.; Mullner, M.; Caruso, F. Multilayered Polymer Capsules With Switchable Permeability. *Polymer* **2014**, *55*, 6451−6459.
(14) Kamat, N. P.; Henry, S. J.; Lee, D.; Hammer, D. A. Single-Vesicle Patterning of Uniform, Giant Polymersomes into Microarrays. *Small* **2013**, *9*, 2272−2276.
(15) Yoshida, R.; Takahashi, T.; Yamaguchi, T.; Ichijo, H. Self-Oscillating Gel. *J. Am. Chem. Soc.* **1996**, *118*, 5134−5135.
(16) Yoshida, R.; Ueki, T. Evolution of self-oscillating polymer gels as autonomous polymer systems. *NPG Asia Mater.* **2014**, *6* (e107), 1−14.
(17) Kuksenok, O.; Dayal, P.; Bhattacharya, A.; Yashin, V. V.; Deb, D.; Chen, I. C.; Van Vliet, K. J.; Balazs, A. C. Chemo-responsive, Self-Oscillating Gels that Undergo Biomimetic Communication. *Chem. Soc. Rev.* **2013**, *42*, 7257−7277.
(18) Deb, D.; Kuksenok, O.; Dayal, P.; Balazs, A. C. Forming self-rotating pinwheels from assemblies of oscillating polymer gels. *Mater. Horiz.* **2014**, *1*, 125−132.

DOI: 10.1021/acs.langmuir.5b01862
Langmuir 2015, 31, 11951−11963

(19) Succi, S. *The Lattice Boltzmann Equation for Fluid Dynamics and Beyond*; Clarendon Press: Oxford, 2001.
(20) Ladd, A. J. C.; Kinney, J. H.; Breunig, T. M. Deformation and Failure in Cellular Materials. *Phys. Rev. E: Stat. Phys., Plasmas, Fluids, Relat. Interdiscip. Top.* **1997**, *55*, 3271−3275.
(21) Alexeev, A.; Verberg, R.; Balazs, A. C. Modeling The Motion of Microcapsules on Compliant Polymeric Surfaces. *Macromolecules* **2005**, *38*, 10244−10260.
(22) Alexeev, A.; Verberg, R.; Balazs, A. C. Designing Compliant Substrates to Regulate the Motion of Vesicles. *Phys. Rev. Lett.* **2006**, *96*, 148103.
(23) Usta, O. B.; Alexeev, A.; Zhu, G.; Balazs, A. C. Modeling Microcapsules that Communicate Through Nanoparticles to Undergo Self-propelled Motion. *ACS Nano* **2008**, *2*, 471−476.
(24) Kolmakov, G. V.; Yashin, V. V.; Levitan, S. P.; Balazs, A. C. Designing Self-propelled Microcapsules for Pick-up and Delivery of Microscopic Cargo. *Soft Matter* **2011**, *7*, 3168−3176.
(25) Chang, K. C.; Hammer, D. A. Adhesive Dynamics Simulations of Sialyl-Lewis^x/E-selectin-Mediated Rolling in a Cell-Free System. *Biophys. J.* **2000**, *79*, 1891−1902.
(26) Krasik, E. F.; Yee, K. L.; Hammer, D. A. Adhesive Dynamics Simulation of Neutrophil Arrest with Deterministic Activation. *Biophys. J.* **2006**, *91*, 1145−1155.
(27) Elowitz, M. B.; Leibler, S. A Synthetic Oscillatory Network of Transcriptional Regulators. *Nature* **2000**, *403*, 335−338.
(28) Chen, S.; Doolen, G. D. Lattice Boltzmann Method for Fluid Flows. *Annu. Rev. Fluid Mech.* **1998**, *30*, 329−364.
(29) Ladd, A. J. C.; Verberg, R. Lattice-Boltzmann Simulations of Particle-Fluid Suspensions. *J. Stat. Phys.* **2001**, *104*, 1191−1251.
(30) Peskin, C. S. The Immersed Boundary Method. *Acta Numer.* **2002**, *11*, 479−517.
(31) Shum, H.; Tripathi, A.; Yeomans, J. M.; Balazs, A. C. Active Ciliated Surfaces Expel Model Swimmers. *Langmuir* **2013**, *29*, 12770−12776.
(32) Goutelle, S.; Maurin, M.; Rougier, F.; Barbaut, X.; Bourguignon, L.; Ducher, M.; Maire, P. The Hill Equation: A Review of Its Capabilities in Pharmacological Modelling. *Fundam. Clin. Pharmacol.* **2008**, *22*, 633−648.
(33) Loinger, A.; Biham, O. Stochastic Simulations of the Repressilator Circuit. *Phys. Rev. E* **2007**, *76*, 051917.
(34) Bhattacharya, A.; Usta, O. B.; Yashin, V. V.; Balazs, A. C. Self-Sustained Motion of a Train of Haptotactic Microcapsules. *Langmuir* **2009**, *25*, 9644−9647.
(35) Gregor, T.; Fujimoto, K.; Masaki, N.; Sawai, S. The Onset of Collective Behavior in Social Amoebae. *Science* **2010**, *328*, 1021−1025.
(36) Kolmakov, G. V.; Schaefer, A.; Aranson, I.; Balazs, A. C. Designing Mechano-responsive Microcapsules that Undergo Self-propelled Motion. *Soft Matter* **2012**, *8*, 180−190.
(37) Zhang, J.; Srivastava, S.; Duffadar, R.; Davis, J. M.; Rotello, V. M.; Santore, M. M. Manipulating Microparticles with Single Surface-immobilized Nanoparticles. *Langmuir* **2008**, *24*, 6404−6408.
(38) Kalasin, S.; Santore, M. M. Engineering Nanoscale Surface Features to Sustain Microparticle Rolling in Flow. *ACS Nano* **2015**, *9*, 4706−4716.
(39) Hammer, D. A.; Robbins, G. P.; Haun, J. B.; Lin, J. J.; Qi, W.; Smith, L. A.; Ghoroghchian, P. P.; Therien, M. J.; Bates, F. S. Leuko-polymersomes. *Faraday Discuss.* **2008**, *139*, 129−141.
(40) Kolmakov, G. V.; Revanur, R.; Tangirala, R.; Emrick, T.; Russell, T. P.; Crosby, A. J.; Balazs, A. C. Using Nanoparticle-filled Micro-capsules for Site-specific Healing of Damaged Substrates: Creating a "Repair-and-Go" System. *ACS Nano* **2010**, *4*, 1115−1123.
(41) Kratz, K.; Narasimhan, A.; Tangirala, R.; Moon, S. C.; Revanur, R.; Kundu, S.; Kim, H. S.; Crosby, A. J.; Russell, T. P.; Emrick, T.; Kolmakov, G.; Balazs, A. C. Probing and Repairing Damaged Surfaces With Nanoparticle-containing Microcapsules. *Nat. Nanotechnol.* **2012**, *7*, 87−90.

DOI: 10.1021/acs.langmuir.5b01862
Langmuir 2015, 31, 11951−11963